Neon Matrix Isolation Electron Spin Resonance and Theoretical Studies of the Various Isotopomers of the CH_3Mg Radical

Allan J. McKinley* and Emmanuel Karakyriakos

Department of Chemistry, The University of Western Australia, Nedlands, Perth, Western Australia 6907

Received: May 12, 2000; In Final Form: July 18, 2000

The $^{12}CH_3Mg$, $^{13}CH_3Mg$, $^{12}CH_3{}^{25}Mg$, $^{12}CD_3{}^{25}Mg$, $^{13}CH_3{}^{25}Mg$ and $^{13}CD_3{}^{25}Mg$ radicals have been isolated in an inert neon matrix at 4.3 K and their electronic structure probed, for the first time, using matrix isolation electron spin resonance (MI-ESR) spectroscopy. These radicals were formed from the reaction of laser-ablated magnesium metal and an appropriately labeled derivative of acetone or methyl iodide. The spin Hamiltonian parameters, $g_\perp = 1.9999(4)$, $A_\perp(^{25}Mg) = -184(1)$ MHz, $A_\perp(^{13}C) = 128(2)$ MHz and $A_\perp(H) = 7(1)$ MHz were determined from an exact diagonalization analysis of the experimental spectra and estimates were derived for $A_{||}(^{25}Mg) = -197(10)$ MHz and $A_{||}(^{13}C) = 180(20)$ MHz assuming $g_{||} = 2.0023$. A model for the bonding in the CH_3Mg radical is derived using this hyperfine data. Comparisons are made between the CH_3Mg radical and other related magnesium and monomethylmetal radicals, MgH, MgOH, CH_3Cd, CH_3Zn, and CH_3Ba. Theoretical nuclear hyperfine coupling constants for the CH_3Mg radical were evaluated using Hartree−Fock single and double excitation configuration interaction (HFSDCI), multireference single and double excitation configuration interaction (MRSDCI) and density functional theory (DFT) ab initio calculations. While these theoretical methods yielded values for $A_{dip}(^{25}Mg)$ and $A_{dip}(^{13}C)$ in agreement with the experimental values, the calculated $A_{iso}(^{25}Mg)$ value was low by 4% (HFSDCI) and 15% (MRSDCI). Whereas the calculated $A_{iso}(^{13}C)$ values were low by 50% (HFSDCI) and 32% (MRSDCI). Unrestricted DFT calculations using the B3PW91 and B3LYP functionals yielded values of $A_{iso}(^{25}Mg)$ low by approximately 15% for both functionals and values of $A_{iso}(^{13}C)$ in agreement with experiment for UB3LYP and low by 10% for UB3PW91. The discrepancy between the calculated and experimental values of $A_{iso}(^{13}C)$ for the CI results is attributed to the limited reference space resulting in an overestimation of the ionic character in the bonding of the CH_3Mg radical.

I. Introduction

Magnesium is the most abundant metal and the seventh most common element yet only two magnesium containing compounds (the MgNC[1] and MgCN[2] radicals) have been detected in circumstellar clouds thus far. It is likely that other magnesium bearing compounds would form in these interstellar and circumstellar clouds but they have yet to be detected.[3] One possible candidate is the CH_3Mg radical, therefore knowledge of the nuclear hyperfine coupling constants in this radical, in particular the ^{25}Mg value, is of considerable interest and may aid in the detection of the CH_3Mg radical if it is present in these clouds. It has also been suggested that CH_3Mg may play an important role in the atmospheric chemistry of gaseous planets such as Jupiter and Neptune.[4]

The wide use and versatility of Grignard reagents for chemical synthesis makes the bonding and electronic structure of the CH_3Mg radical of particular interest. Magnesium containing molecules are of great biological importance, none more so than chlorophyll, the magnesium porphyrin involved in plant photosynthesis. Therefore, knowledge of the bonding and electronic structure in simple magnesium containing radicals such as CH_3Mg may aid in a better understanding of more complex magnesium containing molecules which occur biologically.

* Corresponding author. Fax: +61−8-93801005. E-mail: ajm@chem.uwa.edu.au.

Several spectroscopic studies of the CH_3Mg radical have been performed, however the nuclear hyperfine parameters for the CH_3Mg radical have yet to be determined. Rubino and co-workers have reported the rotationally resolved laser-induced fluorescence (LIF) spectrum ($\tilde{A}^2E \leftrightarrow X^2A_1$ transition)[5] while Salzberg and co-workers have recorded the vibrationally resolved LIF spectrum ($\tilde{A}^2E \leftrightarrow X^2A_1$ transition).[6] Anderson and Ziurys recorded the millimeter/submillimeter spectrum and determined the rotational rest frequencies of the CH_3Mg radical ground state.[7] Recently Barckholtz and co-workers reported the resonance-enhanced multiphoton ionization (REMPI) and zero kinetic energy (ZEKE) photoelectron spectra of the CH_3Mg and CH_3Zn radical.[8] For both species the spin−orbit and vibrational structure of the first excited state ($\tilde{A}^2E$) was resolved and these authors present an "experimental" molecular orbital diagram for these molecules. They also report density functional calculations of the geometry and vibrational frequencies for these radicals.

Bare and Andrews have conducted a matrix isolation infrared study of the products of various reactions of methyl halides and laser ablated magnesium atoms.[9] The primary reaction products studied were CH_3MgF, CH_3MgCl, CH_3MgBr and CH_3MgI. The CH_3Mg radical was not detected in this study. McCaffrey and co-workers have isolated MgH_2 and $HMgCH_3$ in cryogenic matrices and conducted UV−visible absorption/fluorescence, infrared and ESR spectroscopic studies.[10] The MgH_2 and

10.1021/jp001773c CCC: $19.00
Published on Web 09/13/2000

$HMgCH_3$ species were formed by photolysis (450-W Xe arc lamp) of magnesium atoms isolated in hydrogen containing rare gas matrices and methane matrices, respectively. No radicals including CH_3Mg were detected by ESR in these methane matrices either upon deposition or after photolysis. Ab initio studies of the ground state of the CH_3Mg radical have been conducted by Quelch and Hillier,[11] Kaupp et al.[12] and Gardner et al.[13] A correlated ab initio study of the X^2A_1 and $\tilde{A}^2E$ states of the CH_3Mg radical was performed by Woon.[14]

Several magnesium containing radicals have been studied by the MI-ESR technique in argon matrices. Knight and Weltner have reported the ^{25}Mg and H hyperfine coupling constants for MgH,[15] Knight and co-workers have reported the ^{19}F hyperfine couplings for the MgF[16] radical and Brom and Weltner have reported the ^{25}Mg and H hyperfine coupling constants for the MgOH radical.[17] The isotropic and dipolar hyperfine coupling constants for ^{19}F and ^{25}Mg in the MgF radical have been determined from millimeter-wave spectroscopy.[18] For both the MgOH[19] and the MgH[20] radicals the H isotropic and dipolar hyperfine coupling constants have been measured using millimeter-wave spectroscopy. The ^{25}Mg isotropic coupling constant was also determined for the MgOH radical.

Recently, together with Knight's group, we have studied the CH_3Cd[21] and CH_3Zn[22] radicals isolated in rare gas matrices using ESR spectroscopy. Knight has also reported an ESR study of the CH_3Pd[23] radical. Other similar radicals that have been investigated by ESR when trapped in low-temperature matrices include CH_2Cu,[24] CH_3CuH,[25] CH_3GaH[26] and CH_3AlH.[27] Some recent high-resolution gas-phase studies of monomethylmetal species have included CH_3Na,[28] CH_3Cd[29,30] and its cation,[31] CH_3Ca,[32−35] CH_3Sr[36,37] and CH_3Ba.[38] For CH_3Cd, $A_{iso}(^{111}Cd)$ and $A_{dip}(^{111}Cd)$ were measured in a high-resolution electronic excitation experiment.[29] The values of $A_{iso}(H)$ and $A_{dip}(H)$ in the CH_3Ca radical were measured in the ground electronic state using the pump/probe microwave-optical double resonance (PPMODR) technique.[32] The values of $A_{iso}(^{137}Ba)$ and $Q(^{137}Ba)$ for the $^{12}CH_3{}^{137}Ba$ radical in its ground vibrational state have also been determined.[38]

The natural isotopic distribution of magnesium metal is ^{24}Mg (78.99%), ^{25}Mg (10.00%) and ^{26}Mg (11.01%). Of these isotopes only the ^{25}Mg has a nonzero nuclear spin ($I = {}^5/_2$, $\mu = -0.8554$) and thus gives rise to an hyperfine coupling interaction. Radicals containing the ^{24}Mg and ^{26}Mg isotopes ($I = 0$) exhibit no metal hyperfine interaction and produce single overlapping ESR spectra. The magnesium nuclei in these isotopomers will be designated simply as Mg without any specific isotopic label.

II. Experimental Section

The apparatus and procedures used for these experiments have been described in detail elsewhere[21] so only a brief description of the experimental procedure will be given here.

The CH_3Mg radical was generated by the reaction of laser ablated magnesium metal with a methyl precursor. The products of these gas-phase reactions were then isolated in a solid neon matrix at 4.3 K and the CH_3Mg radical identified using ESR. The methyl precursors used were $(^{12}CH_3)_2{}^{12}CO$, $(^{13}CH_3)_2{}^{12}CO$ (Sigma, 98 atom % ^{13}C), $(^{12}CD_3)_2{}^{12}CO$ (Cambridge Isotope Laboratories 99.9 atom % D) and $^{13}CD_3I$ (Aldrich, 99 atom % ^{13}C and D). These precursors were used as received after several freeze−pump−thaw cycles to remove any dissolved air. The neon (Matheson Gas Products, Inc. ultrahigh purity) matrix gas was passed through molecular sieve traps (Linde 5A) at 77 K before use. The magnesium metal target (BDH GPR 99.5% or LR grade 97% by ICP-AES) was ablated using the frequency doubled output of a Nd:YAG laser (Surelite I), 532 nm, 10 mJ per pulse at 10 Hz. The output of the laser was focused to a tight spot (7.5 cm focal length lens) which was continually rastered over the metal surface during the matrix deposition. The gas mixtures were made in situ by introducing the neon and methyl precursor gases directly into the ablation chamber. The methyl precursor gas flow rate into the chamber was monitored by a pressure increase in the line leading to the chamber using a thermocouple gauge and the neon flow rate into the chamber was monitored with a calibrated mass flowmeter (Aalborg GFM 1700). Typical pressure increases with a methyl precursor flow were 5−10 mTorr and on average the neon flow rate was 8 standard cubic centimeters per minute (SCCM). The concentration of the methyl precursor in the neon was estimated to be of the order of 1:1000. The methyl precursor vapor was introduced into the chamber near the magnesium vapor plume while the neon gas was directed toward the deposition target. The total pressure of the system with both the methyl precursor and neon flowing into the ablation chamber was approximately 2×10^{-5} Torr. Background pressure before cooling the cryostat was typically around 8×10^{-8} Torr. The matrix was deposited onto an oxygen free high conductivity (OFHC) copper deposition target which was maintained at 4.3 K by a continuous-flow liquid helium cryostat (Cryo Industries of America RC110). The matrices were deposited over a 1 h period. The ESR spectra were recorded at temperatures between 4.3 and 10.5 K on a Bruker ESP300E spectrometer equipped with a DM4116 cavity.

Spectral analysis was carried out using exact diagonalization of the spin Hamiltonian using the program GEN developed by Knight and co-workers.[39,40] The spin Hamiltonian used was

$$\hat{H} = \beta_e \bar{B}\cdot\hat{g}\cdot\bar{S} + \sum_i (\bar{I}^i\cdot\hat{A}^i\cdot\bar{S} - g_I^i \beta_n \bar{B}\cdot\bar{I}^i)$$

where all symbols have their usual meaning.[41] It was found to be unnecessary to include a term for quadrupole effects involving the ^{25}Mg nucleus in order to obtain agreement, within experimental uncertainty, between the experimental and calculated values of the ESR line positions. The ESR spectral analysis was performed on an IBM RS6000 model 530H computer. The ab initio calculations were performed on the same computer using the MELDF suite of programs[42] and the Gaussian-94 package[43] as well as a Dec Alpha model 500 au computer using the Gaussian-98 package.[44]

III. Results

A. Neon Matrices. Figure 1 shows the ESR spectrum assigned to the neon matrix isolated $^{12}CH_3Mg$ radical formed through the reaction of laser ablated magnesium metal and $(^{12}CH_3)_2{}^{12}CO$. The spectrum was recorded at 9.5 K with a microwave power of 0.1 mW. The expected signal is a 1:3:3:1 quartet due to the three equivalent hydrogen nuclei ($I = {}^1/_2$) in the $^{12}CH_3Mg$ radical. The center of the observed quartet is slightly upfield of g_e and the intensity ratio of the peaks is approximately 1:3:3:1. The "phase-down" line shape of the peaks suggests that the CH_3Mg radical has axial symmetry and that these are the perpendicular peaks arising from radicals whose orientation is perpendicular to the applied field. The parallel peaks, which are expected to be located near g_e, would be broad and weak and were not identified unequivocally due to congestion from other radical signals. The measured perpen-

TABLE 1: Observed ESR Line Positions (Gauss) for the Perpendicular Transitions of the $^{12}CH_3Mg$, $^{13}CH_3Mg$, $^{12}CD_3{}^{25}Mg$, and $^{12}CH_3{}^{25}Mg$ Radicals in a Neon Matrix[a]

$^{12}CH_3Mg$		$^{13}CH_3Mg$			
		$^{13}C:M_I = 1/2$		$^{13}C:M_I = -1/2$	
H:M_J		H:M_J		H:M_J	
3/2	3467.1	3/2	3447.8	3/2	3493.6
1/2	3469.5	1/2	3450.2	1/2	3496.1
−1/2	3472.0	−1/2	3452.6	−1/2	3498.5
−3/2	3474.4	−3/2	*b*	−3/2	*b*

$^{12}CD_3{}^{25}Mg$[c]

$^{25}Mg:M_I = -5/2$ D:M_J	$^{25}Mg:M_I = -3/2$ D:M_J	$^{25}Mg:M_I = -1/2$ D:M_J	$^{25}Mg:M_I = 1/2$ D:M_J	$^{25}Mg:M_I = 3/2$ D:M_J	$^{25}Mg:M_I = 5/2$ D:M_J
3306.8	3369.5	*b*	*b*	3569.6	3634.3

$^{12}CH_3{}^{25}Mg$

$^{25}Mg:M_I = -5/2$ H:M_J		$^{25}Mg:M_I = -3/2$ H:M_J		$^{25}Mg:M_I = -1/2$ H:M_J	$^{25}Mg:M_I = 1/2$ H:M_J	$^{25}Mg:M_I = 3/2$ H:M_J		$^{25}Mg:M_I = 5/2$ H:M_J	
3/2	3301.1	3/2	3364.1	*b*	*b*	3/2	3561.7	3/2	3630.2
1/2	3303.6	1/2	3366.5			1/2	3564.2	1/2	3632.7
−1/2	3306.0	−1/2	3368.9			−1/2	3566.6	−1/2	3635.3
−3/2	3308.2	−3/2	3371.4			−3/2	3569.2	−3/2	3637.6

[a] All matrices were annealed and the ESR spectra recorded at 9.5 K. The calculated line positions, determined by an exact diagonalization analysis using the magnetic parameters in Table 2, agree with these line positions within the experimental uncertainty which was ±0.3 G for the lines not exhibiting magnesium hyperfine splitting (hfs) and ±0.4 G for the lines exhibiting magnesium hfs. The microwave frequency was 9714.61(1) MHz for $^{12}CH_3Mg$, 9725.12(1) MHz for $^{13}CH_3Mg$, 9716.26(3) MHz for $^{12}CD_3{}^{25}Mg$, and 9714.65(4) MHz for $^{12}CH_3{}^{25}Mg$. The perpendicular lines have $\Theta = 90°$. [b] Peaks obscured by signals from other radicals. [c] The expected septets were unresolved and appeared as broad peaks so the line positions were taken from the base of these peaks.

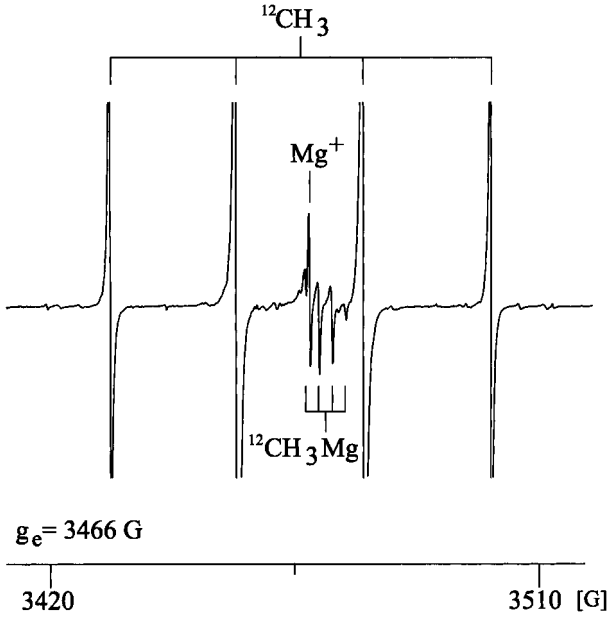

Figure 1. The ESR spectrum of the $^{12}CH_3Mg$ radical isolated in a neon matrix at 9.5 K. The spectrum was recorded with a microwave power of 0.1 mW and at a microwave frequency of 9714.61(1) MHz. The $^{12}CH_3Mg$ radical was generated from the reaction of laser ablated magnesium metal with $(^{12}CH_3)_2{}^{12}CO$. The $^{12}CH_3Mg$ radical spectrum consists of a 1:3:3:1 "phase down" quartet of lines. Only the perpendicular transitions of the radical are observed. The parallel transitions are expected to be weaker and were not observed. The ESR peaks due to the $^{12}CH_3$ radical and Mg^+ ion are also labeled.

dicular line positions for this radical are given in Table 1. These line positions were fitted within their experimental uncertainty with an exact diagonalization analysis of the spin Hamiltonian using the parameters given in Table 2. For this analysis the $g_{\|}$ value was assumed to be 2.0023. The ESR signals due to the $^{12}CH_3$ radical and Mg^+ ion are also labeled in Figure 1.

TABLE 2: Magnetic Parameters (MHz) of the Isotopomers of the CH_3Mg Radical[a]

	$g_\perp$[b]	$A_\perp$	$A_{\|}$	A_{iso}[c,d]	A_{dip}[c,d]
H[e]	1.9999(4)	7(1)			−7(1)
^{13}C	1.9999(4)	128(2)	180(20)	145(8)	17(10)
^{25}Mg	1.9999(4)	−184(1)	−197(10)	−188(4)	−4(5)

[a] The uncertainties on the parameters are based on the change required to shift at least one of the simulated line positions outside the range of the experimental line position uncertainty or the change required to significantly alter the simulated line shape from the experimental line shape. [b] $g_{\|}$ is assumed equal to 2.0023. [c] A_{iso} and A_{dip} were calculated from standard expressions.[41] [d] These experiments cannot determine the sign of A_{iso} or A_{dip}; the signs given are based on the theoretical values. [e] A_{dip} for hydrogen is small; hence A_{iso} is assumed to be equal to $A_\perp$.

At 4.3 K two additional doublets flanking each line of the central doublet of the CH_3Mg quartet were present in the ESR spectrum. These additional lines weaken relative to the quartet as the temperature is raised from 4.3 K becoming indiscernible at 6.0 K. On recooling they grow in again reversibly. We have observed a similar phenomena for the CH_3Cd[21] and CH_3Zn[22] radical and attributed the extra lines to tunneling effects associated with restricted motion of the radical in the matrix. Interestingly the temperatures when these peaks were lost in neon matrices were 10.5 K for CH_3Cd, 8.0 K for CH_3Zn and 6.0 K for CH_3Mg.

The assignment of the quartet in Figure 1 to the $^{12}CH_3Mg$ radical can be confirmed by identifying the ^{25}Mg hyperfine ($I = 5/2$) splitting for the $^{12}CH_3{}^{25}Mg$ radical. The ESR spectrum for the $^{12}CH_3{}^{25}Mg$ radical will consist of a widely spaced sextet of quartets with the quartets each having the same splitting as that observed for the $^{12}CH_3Mg$ radical. The sextet is expected to have an intensity that is at best 1.7% of the signal intensity of the $^{12}CH_3Mg$ radical given the 10% natural abundance of ^{25}Mg which has $I = 5/2$. In fact depending on the relative g and A anisotropy the intensity of each line of the sextet will vary. The center trace of Figure 2 shows the ESR spectrum of four

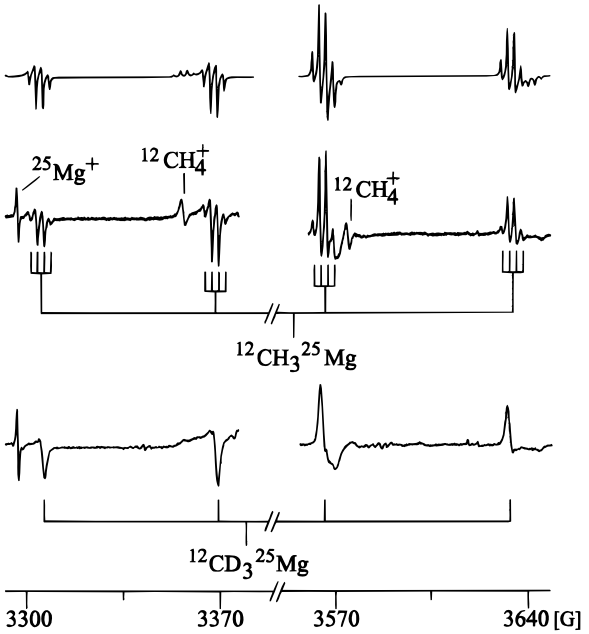

Figure 2. The ESR spectra of the ^{25}Mg hyperfine for the $^{12}CH_3{}^{25}Mg$ and $^{12}CD_3{}^{25}Mg$ radical in a neon matrix at 9.5 K recorded at a microwave power of 0.1 mW. The center trace shows the ESR spectrum of the $^{12}CH_3{}^{25}Mg$ radical recorded with a microwave frequency of 9714.65(4) MHz. The methyl source used was $(^{12}CH_3)_2{}^{12}CO$. The lower trace shows the ESR spectrum of the $^{12}CD_3{}^{25}Mg$ radical with a microwave frequency that has been normalized to match the center trace. The methyl source used was $(^{12}CD_3)_2{}^{12}CO$. The top trace shows the simulated ESR spectrum of the $^{12}CH_3{}^{25}Mg$ radical using the appropriate magnetic parameters from Table 2. The $^{25}Mg{:}M_I = -1/2$ and $1/2$ set of peaks for both radicals were obscured by peaks from other radicals and have been omitted. The peaks of the $^{25}Mg^+$ and $^{12}CH_4{}^+$ ions occurring in this field range are labeled.

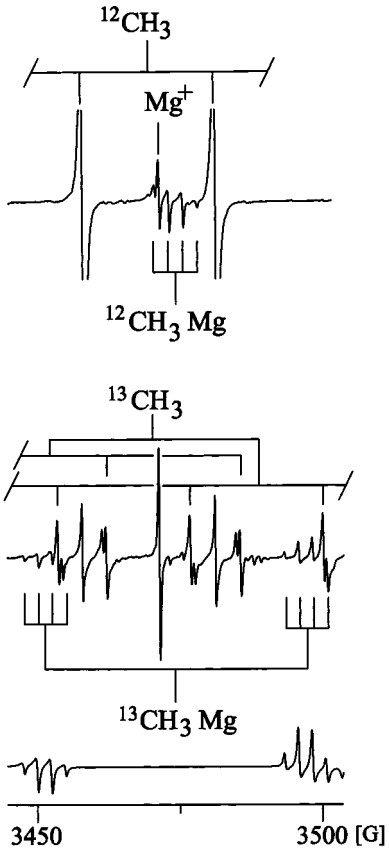

Figure 3. The ESR spectra of the ^{13}C hyperfine of the $^{13}CH_3Mg$ radical isolated in a neon matrix at 9.5 K. The center trace shows the ESR spectrum of the $^{13}CH_3Mg$ radical recorded at a microwave power of 0.01 mW and with a microwave frequency of 9725.12(1) MHz. The $H{:}M_J = -3/2$ peaks for both sets of quartets were obscured by $^{13}CH_3$ radical peaks. The radical was generated from the reaction of laser ablated magnesium metal with $(^{13}CH_3)_2{}^{12}CO$. The top trace shows the $^{12}CH_3Mg$ radical ESR spectrum for comparison. The microwave frequency was normalized to match the center trace. The lower trace shows the simulated ESR spectrum for the $^{13}CH_3Mg$ radical using the appropriate magnetic parameters in Table 2. Background radicals $^{12}CH_3$, $^{13}CH_3$ and Mg^+ ions are labeled.

of the six expected quartets for the $^{12}CH_3{}^{25}Mg$ radical ($^{25}Mg{:}M_I = -5/2$, $-3/2$, $3/2$ and $5/2$) in a neon matrix at 9.5 K. Unfortunately the $^{25}Mg{:}M_I = -1/2$ and $1/2$ quartets which are the closest to g_e are totally obscured by the significantly more intense $H{:}M_J = 3/2$ and $-3/2$ $^{12}CH_3$ radical peaks. As expected the spacing between the peaks in these four quartets is the same as the spacing in the $^{12}CH_3Mg$ radical quartet. The intensities of these quartets, assigned to the $^{12}CH_3{}^{25}Mg$ radical, relative to the $^{12}CH_3Mg$ radical quartet, range from approximately 1.1% to 1.3% which is consistent with the expected maximum intensity ratio of 1.7%.

As the parallel lines for the $^{12}CH_3Mg$ radical were not observed the $A_{||}(^{25}Mg)$ value and its associated error had to be estimated from an analysis of the position and line shape of the perpendicular peaks. A series of simulations of the ESR spectrum were conducted and limits placed on the range of $A_{||}(^{25}Mg)$ values that matched the experimental spectrum. While the $A_{||}(^{25}Mg)$ value had little effect on the perpendicular line positions the line shape of the $^{25}Mg{:}M_I = 3/2$ peaks did show a reasonable sensitivity to varying the $A_{||}(^{25}Mg)$ value. The simulated ESR spectrum, performed with an exact diagonalization of the spin Hamiltonian using the appropriate magnetic parameters listed in Table 2, for the $^{12}CH_3{}^{25}Mg$ radical is shown in the top trace of Figure 2. The observed line positions for the $^{12}CH_3{}^{25}Mg$ radical quartets are given in Table 1. The simulated and observed line positions agree within experimental error. The ESR signals due to the $^{25}Mg^+$ [17] and $^{12}CH_4{}^+$ [45] ions appearing in this field range are also labeled in Figure 2.

The lower trace in Figure 2 shows the ESR spectrum of the $^{12}CD_3{}^{25}Mg$ radical in a neon matrix at 9.5 K. This radical was formed by the reaction of $(^{12}CD_3)_2{}^{12}CO$ and laser ablated magnesium. As the deuterium hyperfine coupling constant is approximately a factor of 6.5 smaller[41] than the hydrogen value the deuterium hyperfine coupling was not resolved and the ESR spectrum consisted of a sextet from the ^{25}Mg coupling with each line of the sextet positioned at the center of the hydrogen quartet in the $^{12}CH_3{}^{25}Mg$ spectrum. As in the $^{12}CH_3{}^{25}Mg$ radical case the $^{25}Mg{:}M_I = -1/2$ and $1/2$ set of peaks for the $^{12}CD_3{}^{25}Mg$ radical were obscured by two of the background $^{12}CH_3$ radical peaks.

To further confirm the assignment of the $^{12}CH_3Mg$ radical quartet $(^{13}CH_3)_2{}^{12}CO$ and laser ablated magnesium were reacted to form the $^{13}CH_3Mg$ radical. Substitution of the ^{12}C ($I = 0$) for a $^{13}C(I = 1/2)$ in the $^{12}CH_3Mg$ radical split the $^{12}CH_3Mg$ radical quartet about its center into a pair of quartets of equal intensity. The center trace of Figure 3 shows the ESR spectrum at 9.5 K of the $^{13}CH_3Mg$ radical in a neon matrix. The ESR spectrum of the $^{12}CH_3Mg$ radical is given in the top trace of Figure 3 for comparison. The two quartets observed have almost equal intensities and the spacing between the peaks in the quartets is the same as the spacing in the $^{12}CH_3Mg$ radical quartet. Because of overlap with the $^{13}CH_3$ radical peaks the $H{:}M_J = -3/2$ peaks of the lower field and higher field quartets

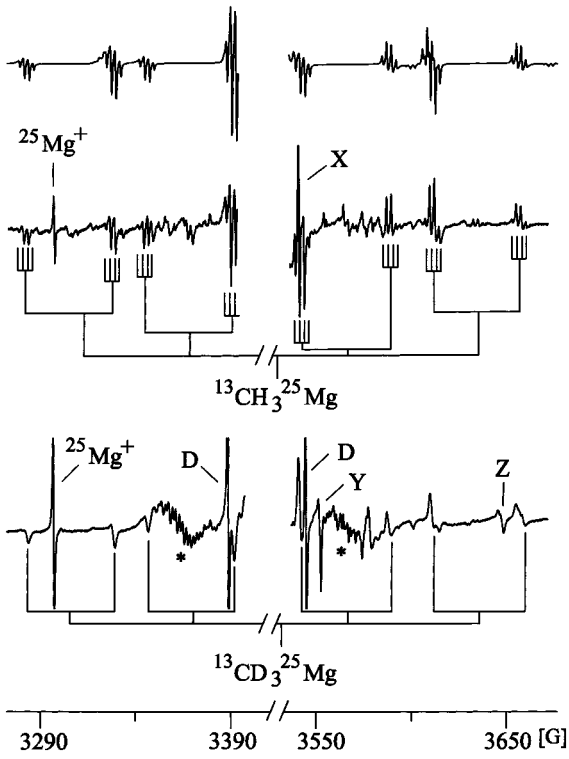

Figure 4. The ESR spectra of various isotopomers of the $^{12}CH_3{}^{25}Mg$ radical in neon at 9.5 K and recorded at a microwave power of 0.1 mW. The lower trace shows the ESR spectrum of the $^{13}CD_3{}^{25}Mg$ radical recorded with a microwave frequency of 9716.65(3) MHz. The center trace shows the ESR spectrum of the $^{13}CH_3{}^{25}Mg$ radical with a microwave frequency that was normalized to match the lower trace. The methyl sources used were $(^{13}CH_3)_2{}^{12}CO$ and $^{13}CD_3I$. The peaks of the D radical, $H^{13}CD_3{}^+$ (labeled as *, see text) and $^{25}Mg^+$ ions occurring in this field region are labeled. The top trace shows the simulated ESR spectrum for the $^{13}CH_3{}^{25}Mg$ radical using the appropriate magnetic parameters from Table 2. The peaks labeled X, Y and Z are due to unknown species (see text).

were not observed. The observed line positions for the $^{13}CH_3Mg$ radical are given in Table 1. Peaks due to Mg^+ ions, $^{13}CH_3$ and $^{12}CH_3$ radicals are labeled in the center trace of Figure 3. The lower trace of Figure 3 is the simulated spectrum for the $^{13}CH_3Mg$ radical calculated using exact diagonalization of the spin Hamiltonian and the appropriate parameters in Table 2. The $A_{||}(^{13}C)$ value and its associated error were estimated by the same method as used for the $A_{||}(^{25}Mg)$ value discussed above.

As a final confirmation of the assignment of these ESR signals the $^{13}CH_3{}^{25}Mg$ and $^{13}CD_3{}^{25}Mg$ radicals were studied. The $^{13}CH_3{}^{25}Mg$ radical was formed by reacting $(^{13}CH_3)_2{}^{12}CO$ with laser ablated magnesium and the $^{13}CD_3{}^{25}Mg$ radical was formed by using $^{13}CD_3I$ instead of $(^{13}CH_3)_2{}^{12}CO$. The center trace of Figure 4 shows the ESR spectrum of the $^{13}CH_3{}^{25}Mg$ radical in a neon matrix at 9.5 K. Substituting ^{13}C for ^{12}C in the $^{12}CH_3{}^{25}Mg$ radical splits all the quartets in Figure 2 into pairs of quartets as seen in the center trace of Figure 4. The magnitude of the ^{13}C hyperfine splitting between the pairs of quartets matches the ^{13}C hyperfine splitting observed for the $^{13}CH_3Mg$ radical in Figure 3. The spacing between the peaks in the quartets themselves is also equivalent. The H:$M_J = -3/_2$ peak for the highest field quartet of the low field set has been omitted as it was masked by the low field line of the HCO radical[41] which was significantly more intense. The lower trace of Figure 4 shows the ESR spectrum of the $^{13}CD_3{}^{25}Mg$ radical in a neon matrix at 9.5 K. Substitution of the hydrogen nuclei by deuterium nuclei in the radical results in the collapse of the hydrogen quartet into a single line as discussed above. So the spectrum consists of a sextet of doublets with each line positioned at the center of the hydrogen quartet of the $^{13}CH_3{}^{25}Mg$ radical. Both the $^{13}CH_3{}^{25}Mg$ and $^{13}CD_3{}^{25}Mg$ radical peaks show an analogous change in line shape from low to high field and all corresponding sets of peaks have similar relative intensities. Note that the $^{13}CH_3Mg$ radical spectrum also exhibited this change in line shape from low to high field. The top trace of Figure 4 is the simulated $^{13}CH_3{}^{25}Mg$ radical spectrum calculated from an exact diagonalization of the spin Hamiltonian using the parameters in Table 2. The parameters used for this simulation were determined from the $^{12}CH_3Mg$, $^{13}CH_3Mg$ and $^{12}CH_3{}^{25}Mg$ radicals and were not adjusted to simulate the $^{13}CH_3{}^{25}Mg$ radical spectrum. The good agreement observed between the experimental and simulated spectrum for the $^{13}CH_3{}^{25}Mg$ radical without refinement of the various hyperfine coupling parameters is a confirmation of the values determined.

Several signals from other radicals are labeled in Figure 4. The peak labeled X in the center trace was only formed when laser ablated magnesium metal was reacted with $(^{13}CH_3)_2{}^{12}CO$. The peaks labeled Y and Z in the lower trace were only observed when laser ablated magnesium metal was reacted with a methyl precursor that contained iodine. The $H^{13}CD_3{}^+$ ion labeled with an asterisk in the lower trace of Figure 4 was observed in the experiments involving $^{13}CD_3I$. These peaks were identified by comparison with the known hyperfine splitting of other $CH_4{}^+$ isotopomers.[45] All four of the expected septets were observed but only two occurred in this field range. Each peak of the septets shows a slight splitting, presumably due to site effects in the matrix. Peaks due to the $^{12}CH_3{}^{25}Mg$ radical are also present in the center and lower traces of Figure 4.

These experiments alone cannot determine the signs of the ^{25}Mg, ^{13}C or H hyperfine coupling constants, the signs given in Table 2 are all based on the theoretical predictions.

B. Theoretical Results. Ab initio calculations were conducted for the X^2A_1 state of CH_3Mg radical as part of this experimental investigation. The CH_3Mg geometry was evaluated in C_{3v} symmetry with Gaussian 94 [43] at the full second-order Møller−Plesset (MP2) level using the uncontracted (12s 8p 1d) cc-pVDZ basis set for magnesium[46] and the uncontracted Dunning DZP sets[47] for carbon (9s 5p 1d) and hydrogen (4s 1p). The optimized geometry was $R_{Mg-C} = 2.114$ Å, $R_{C-H} = 1.095$ Å, and $\angle H-C-Mg = 111.0°$. Unrestricted density functional theory (DFT) calculations with Gaussian 98[44] were also conducted using the unrestricted UB3LYP[48] and UB3PW91[49] functionals and the same basis set as described above. The CH_3Mg geometry determined was $R_{Mg-C} = 2.138$ Å, $R_{C-H} = 1.093$ Å and $\angle H-C-Mg = 110.1°$ for UB3LYP and $R_{Mg-C} = 2.126$ Å, $R_{C-H} = 1.094$ Å and $\angle H-C-Mg = 111.6°$ for B3PW91. The MP2 geometry shows reasonable agreement with the experimentally determined values reported by Anderson and Ziurys[7] of $R_{Mg-C} = 2.11$ Å from the millimeter/submillimeter wave spectrum and that reported by Rubino and co-workers[5] of $R_{Mg-C} = 2.102$ Å and $\angle H-C-Mg = 110.7°$ assuming $R_{C-H} = 1.105$ Å from the LIF spectrum. While the DFT results yield a Mg−C bond length significantly longer than the experimental values.

There have been several earlier theoretical studies on the CH_3Mg radical geometry. Barckholtz and co-workers[8] reported $R_{Mg-C} = 2.148$ Å, $\angle H-C-Mg = 109.6°$ and $R_{C-H} = 1.100$ Å from a DFT calculation using the Becke-Perdew gradient-corrected functional and $R_{Mg-C} = 2.108$ Å, $\angle H-C-Mg = 109.6°$ and $R_{C-H} = 1.102$ Å from a DFT calculation using the

TABLE 3: Comparison of the Experimental and Theoretical Magnetic Parameters (MHz) of the CH_3Mg Radical

	^{25}Mg		^{13}C		H	
	A_{iso}	A_{dip}	A_{iso}	A_{dip}	A_{iso}	A_{dip}
exp[a]	−188(4)	−4(5)	145(8)	17(10)	−7(1)	
theor[b]						
HFSDCI[c]	−181	−5.5	73	8	−1.8	[−0.9, −4.6, 5.5][f]
MRSDCI[d]	−159	−5.6	99	12	−3.0	[−1.1, −6.2, 7.3][f]
UB3LYP[e]	−157	6.0	149	19	−3.9	[−2.0, −9.2, 11.2][f]
UB3PW91[e]	−161	5.8	130	16	−3.9	[−1.6, −8.1, 9.7][f]

[a] This work. [b] This work. The basis sets used were the uncontracted (12s 8p 1d) cc-pVDZ set for magnesium[46] and the uncontracted Dunning DZP sets for carbon (9s 5p 1d) and hydrogen (4s 1p).[47] [c] All single excitations from the Hartree−Fock solution and those double excitations which exceeded an energy threshold of $5 \times 10-8$ hartree were retained in the CI calculation. The HFSDCI calculation included 63 082 spin-adapted configurations, had a sum of squares of the coefficients in the reference space of 0.93 and a total CI energy of −239.5896 hartree. [d] The MRSDCI calculation used 75 reference configurations chosen on the basis of their CI coefficient from the HFSDCI calculation. The MRSDCI calculation included 611 805 spin-adapted configurations, had a sum of squares of the coefficients in the reference space of 0.95 and a total CI energy of −239.5999 hartree. All single excitations from the reference space and those double excitations which exceeded an energy threshold of 5×10^{-8} hartree were retained in the CI calculation. [e] DFT calculations performed using GAUSSIAN 98.[44] [f] The rotation angle between molecular axes and the principal magnetic axes was 41° (HFSDCI), 42° (MRSDCI), 36° (UB3LYP), and 38° (UB3PW91).

local density approximation functional and a STO triple-ζ basis set which included polarization functions and frozen core approximation for the innermost carbon and magnesium orbitals. Woon[14] reported a geometry of $R_{Mg-C} = 2.109$ Å, $R_{C-H} = 1.094$ Å and $\angle H-C-Mg = 111.0°$ using the restricted coupled-cluster method (RCCSD(T)) and the cc-pCVTZ (core valence) basis sets on magnesium and carbon and the cc-pVTZ on hydrogen. Gardner and co-workers[13] reported $R_{Mg-C} = 2.12$ Å, $R_{C-H} = 1.10$ Å, $\angle H-C-Mg = 111°$ and $\angle H-C-H = 108°$ from a full MP2/6-311** calculation.

We evaluated the magnetic hyperfine coupling constants for the CH_3Mg radical from Hartree−Fock singles and doubles configuration interaction (HFSDCI) and multireference singles and doubles configuration interaction (MRSDCI) calculations using the MELDF suite of programs.[42] The same basis sets used in the above Gaussian 94 geometry calculation were used for these calculations. The HFSDCI calculations included all single excitations from the Hartree−Fock configuration and those double excitations with an energy exceeding a threshold energy of 5×10^{-8} hartree. The MRSDCI calculation used 75 reference configurations, chosen on the basis of the CI coefficient contribution to the HFSDCI calculation, as the reference space for the CI calculation. For comparison the magnetic hyperfine coupling constants for the CH_3Mg radical were also evaluated from DFT calculations with the UB3LYP and UB3PW91 functionals using Gaussian 98 suite of programs[44] at the geometry optimized for each functional listed above. The results of these calculations are presented with the experimental results in Table 3.

IV. Discussion

A. Comparison between Theoretical and Experimental Results. Table 3 shows the comparison between the experimental neon matrix ESR hyperfine coupling constants and the theoretical results from the HFSDCI, MRSDCI, UB3LYP and UB3PW91 calculations for the CH_3Mg radical. The experimental A_{iso} and A_{dip} values were calculated using the following standard expressions:[41]

$$A_{iso} = \frac{2A_{\perp} + A_{||}}{3}$$

$$A_{dip} = A_{iso} - A_{\perp}$$

where

$$A_{iso} = 8\pi g_e g_n \beta_e \beta_n |\psi(0)^2|/3$$

$$A_{dip} = g_e g_n \beta_e \beta_n \langle 3\cos^2\theta - 1)/2r^3 \rangle$$

We have assumed $A_{\perp}$(H) is equal to A_{iso}(H). Even though the hydrogen nuclei do not lie on the 3-fold axis and the observed value of $A_{\perp}$ is the projection onto that axis, the A_{dip}(H) value for hydrogen is expected to be small and rotation of the radical in the matrix about this axis will average the dipolar contribution to the hydrogen hyperfine coupling to zero.

The agreement between the $A_{iso}(^{25}Mg)$ and $A_{dip}(^{25}Mg)$ values from the HFSDCI calculation with the experimental values is excellent. The calculated $A_{dip}(^{25}Mg)$ value agreeing within the experimental uncertainty while the calculated $A_{iso}(^{25}Mg)$ value is barely outside this range. The $A_{dip}(^{25}Mg)$ value from the MRSDCI calculation agrees well with the experimental value but the agreement between the experimental $A_{iso}(^{25}Mg)$ value and the MRSDCI value is less satisfactory. The theoretical values of $A_{iso}(^{13}C)$ from both the HFSDCI and MRSDCI calculations are significantly lower than the experimental value. The theoretical $A_{iso}(^{13}C)$ for the HFSDCI calculation is low by almost 50% and low by approximately 32% for the MRSDCI calculation. The theoretical $A_{dip}(^{13}C)$ values from the HFSDCI and MRSDCI calculation agree with the experimental value within the experimental uncertainty. Detailed comparison between the theoretical values of A_{iso}(H) is complicated by the assumption that the experimental value of $A_{\perp}$(H) is equal to A_{iso}(H), but it would appear either the HFSDCI and MRSDCI values are low or that there is a significant dipolar contribution to the experimental value of $A_{\perp}$(H).

In earlier studies of the CH_3Cd and CdH radicals[21] and CH_3Zn and ZnH radicals[22] we also observed that the HFSDCI and MRSDCI calculations yielded low A_{iso} values for the nucleus bonded to the metal. We attributed[22] this observation to the CI calculations, with limited reference space, not getting the correct amount of mixing between the three configurations, namely $M(ns^2)$ CH_3, $M(sp)-CH_3$ and M^+ CH_3^-. We also found that for $A_{iso}(^{13}C)$ and A_{iso}(H) in the CH_3Zn radical and A_{iso}(H) in the ZnH radical better agreement with experiment was achieved with the UB3PW91 method. The results of UB3LYP and UB3PW91 calculations of the hyperfine coupling constants for the CH_3Mg radical are also shown in Table 3. Both methods yield similar values for $A_{iso}(^{25}Mg)$ and $A_{dip}(^{25}Mg)$ in agreement with the MRSDCI results. The $A_{iso}(^{25}Mg)$ values are low compared with the experimental value and the $A_{dip}(^{25}Mg)$ agrees with the experimental value within the experimental uncertainty. Both methods also yield the same value of A_{iso}(H) which is marginally larger than the MRSDCI value but less than experimental value. For $A_{iso}(^{13}C)$ and $A_{dip}(^{13}C)$ both methods yield larger values than the MRSDCI results. The $A_{dip}(^{13}C)$ value from both methods agrees with the experimental value within the experimental uncertainty, and the value of $A_{iso}(^{13}C)$ from the UB3LYP calculation agrees with the experimental value while the value of $A_{iso}(^{13}C)$ from the UB3PW91 calculation is

TABLE 4: Comparison of the Experimental[a] and the Theoretical Spin Densities for the CH_3Mg Radical and the Experimental Spin Densities for the MgH and MgOH Radicals

	^{25}Mg		^{13}C		H	Total
	$a_1^2\chi(3s)$	$a_2^2\chi(3p_z)$	$a_3^2\chi(2s)$	$a_4^2\chi(2p_z)$	$a_5^2\chi(1s)$	$\sum a_i^2$
			CH_3Mg[b]			
exp						
FACM	0.40(1)	0.56(64)	0.04(1)	0.16(9)	−0.005(1)	1.14(76)
g shift		0.59(1)				
theor						
MRSDCI[c]	0.55	0.24[d]	0.03	0.13[e]	−0.001	0.96
			MgH			
MI-ESR[f]	0.47(1)	0.38(15)			0.21(1)	1.06(17)
gas phase[g]	*h*	*h*			0.22(1)	
			MgOH			
MI-ESR[i]	0.64(1)	0.51(12)			0.008(2)	1.16(14)
gas phase[j]	0.64(1)	*h*			0.005(3)	

[a] The experimental values were calculated using the free atom comparison method, (FACM) see text. Because of the approximate nature of the FACM the errors are the larger of either ±0.01 or the standard propagated error based on the uncertainty in the experimental A_{iso} or A_{dip} values. [b] This work. [c] Mulliken gross spin populations from the MRSDCI calculation with 75 reference configurations and a threshold of retaining double excitations in the CI of 5×10^{-8} hartree. [d] This is the gross spin population for the magnesium $\chi(3p_z)$. The $\chi(3p_x)$ and $\chi(3p_y)$ values are 0.0006. [e] This is the gross spin population for the carbon $\chi(2p_z)$. The $\chi(2p_x)$ and $\chi(2p_y)$ values are 0.0046. [f] Determined from the hyperfine coupling constant values in ref 15 using FACM. [g] Determined from the hyperfine coupling values in ref 20 using FACM. [h] Not determined in this study. [i] Determined from the hyperfine coupling constant values in ref 17 using FACM. [j] Determined from the hyperfine coupling constant values in ref 19 using FACM.

lower by 10% but still closer than that obtained from the MRSDCI calculation.

Interestingly the variation of the calculated dipole moment for the CH_3Mg radical with the various theoretical approaches shows a trend which is consistent with the CI calculations overestimating the ionic character of the magnesium−carbon bond. The values are: 1.095 D (HFSDCI), 0.8214 D (MRSDCI), 0.7604 D (UB3LYP) and 0.7903 D (UB3PW91).

B. Electronic Structure of the CH_3Mg Radical. The $\Delta g_\perp$ value for the CH_3Mg radical is −0.00239 where $\Delta g_\perp = g_\perp - g_e$. This deviation is due to spin−orbit coupling between the X^2A_1 and $\tilde{A}^2E$ states and can be quantified[41] by the following approximate relationship $\Delta g_\perp = -2\zeta_{3p}a_2^2/\Delta E$ where ζ_{3p} is the metal spin−orbit parameter (40.4(7) cm^{-1} for magnesium[50]), a_2^2 is the $3p_z$ character of the HOMO and ΔE is the energy separation between the ground and the first excited ^2E state.[51] Given that ΔE ($\tilde{A}^2E \leftarrow X^2A_1$) has a value of 20030.2963(16) cm^{-1} [5] and $\Delta g_\perp = -0.00239$, a_2^2 is calculated to be 0.59(1). This value agrees with the FACM result of 0.56(64) described in the next section and given the large experimental uncertainty in the FACM result it provides an important alternative derivation of the *3*p character of the CH_3Mg HOMO.

C. Bonding in the CH_3Mg Radical. A linear combination of atomic orbitals (molecular orbitals) or LCAO-MO model of the highest occupied molecular orbital (HOMO) of the CH_3Mg radical would be as follows:

$$\Psi(X^2A_1) = a_1\chi(\text{Mg 3s}) + a_2\chi(\text{Mg 3p}_z) + a_3\chi(\text{C 2s}) + a_4\chi(\text{C 2p}_z) + a_5\chi(\text{H 1s})$$

where $\Psi(X^2A_1)$ is the molecular wave function of the HOMO, χ(Mg 3s) etc. represent the atomic orbitals and the a_1 etc. represent the coefficients of each atomic orbital contributing to the HOMO. The squares of the coefficients for each atomic orbital, ie. spin densities, can be estimated using the free atom comparison method (FACM). This method involves taking a ratio of the experimental molecular values of A_{iso} and A_{dip} for each nucleus with their respective atomic values. Note that FACM does not take polarization effects into account. For carbon and hydrogen the standard theoretical atomic parameters[41] were used to evaluate the orbital characters. For magnesium the atomic values of A_{iso} and A_{dip} were derived from the hyperfine coupling constants a_s and $a_{3/2}$ which have been evaluated from level crossing experiments involving emission from the first excited $^1P_1$ state of ^{25}Mg atoms in the gas phase by Kluge and Sauter.[52] The a_s parameter is equivalent to the atomic A_{iso} value. However A_{dip} cannot be determined from $a_{3/2}$ alone. Fortunately the $\langle r_{sC} - 3\rangle_{3p}$ (^3P) and $\langle r_l - 3\rangle_{3p}$ (^1P) values for ^{25}Mg have been derived experimentally.[54] Using these values and the following equations:[41]

$$P_L = g_e g_n \beta_e \beta_n \langle r_l^{-3}\rangle_{3p}$$

$$P_S = g_e g_n \beta_e \beta_n \langle r_{sC}^{-3}\rangle_{3p}$$

P_L and P_S can be determined and then along with $a_{3/2}$ can be substituted into the following equations reported by Ammeter and Schlosnagle to determine the $a_{1/2}$ value:[53]

$$a_{3/2} = \frac{2}{3}P_L - \frac{2}{15}P_S + \frac{1}{3}A_0$$

$$a_{1/2} = \frac{4}{3}P_L + \frac{4}{3}P_S - \frac{1}{3}A_0$$

Once the $a_{1/2}$ and $a_{3/2}$ values are known they can be used to derive an estimate for the atomic A_{dip} value of magnesium using the following relations:[53]

$$\bar{P} = \frac{5}{16}(a_{1/2} + a_{3/2})$$

$$A_{dip} = \frac{2}{5}\bar{P}$$

This approximation neglects relativistic effects but for light atoms this is acceptable.[53] The terms and symbols in all of the above equations have their usual meaning. The magnesium atomic values that were obtained from this procedure were −472.5 MHz for A_{iso} and −7.8(4) MHz for A_{dip}.

The spin densities derived from the FACM for the CH_3Mg radical are shown in Table 4 along with the results of a Mulliken spin population analysis on the MRSDCI wave functions discussed previously and the value of a_2^2 derived from the $\Delta g_\perp$

value discussed in the previous section. The FACM value of a_2^2 has a large uncertainty due the difficulty of determining the value of $A_{||}(^{25}Mg)$ accurately. Fortunately the $\Delta g_\perp$ value provides an alternative route to the value of a_2^2. The theoretical spin densities overestimate the magnesium 3s orbital character and underestimate the magnesium $3p_z$ orbital contribution to the HOMO. This is consistent with this MRSDCI calculation overestimating the contribution of the $M^+ CH_3^-$ configuration to the HOMO as discussed above. We observed this same trend for MRSDCI calculations on both the CH_3Cd[21] and CH_3Zn[22] radicals. Also shown in Table 4 are the equivalent spin density results for the MgH and MgOH radicals which were derived from the experimental hyperfine parameters determined in MI-ESR experiments reported in refs 15 and 17, respectively using the same atomic parameters as those used for the CH_3Mg radical. For the MgOH radical the oxygen hyperfine was not observed so the spin density on the oxygen could not be evaluated, but it is expected to be small. For comparison the spin densities derived in the same way from the hyperfine coupling constants that have been measured from the gas-phase rotational studies for the MgH[20] and MgOH[19] radicals are also shown in Table 4. Only a limited comparison is possible between the data from the MI-ESR and the gas phase millimeter-wave experiments as the only ^{25}Mg hyperfine coupling constant which has been evaluated in the gas phase is the $A_{iso}(^{25}Mg)$ value for MgOH. However those values that have been determined by both methods agree within the experimental uncertainty. Because of the paucity of gas-phase hyperfine data few comparisons of this type are possible and it is interesting to note here that in an earlier study[21] of the CH_3Cd radical the neon matrix MI-ESR ^{111}Cd hyperfine coupling constants agreed within 5% of the gas-phase values.[29]

In these magnesium species for a purely ionic bond the HOMO is expected to be entirely magnesium 3s orbital in character as the unpaired electron would be entirely localized on the magnesium as in the Mg^+ ion whereas for a covalent bond the HOMO will be expected to have magnesium 3s and $3p_z$ character. It is clear from Table 4 that the experimental spin densities for the CH_3Mg and MgH radical are very similar which implies that the magnesium−carbon and magnesium−hydrogen bonds are similar in the two radicals. The total spin density on the magnesium is 84(11) % for the CH_3Mg radical (using the value of a_2^2 from the *g*-shift expression) and 80(28) % for the MgH radical. The magnesium 3s character for the CH_3Mg radical is slightly lower than that for the MgH radical but as the MgH experiments were performed in an argon matrix this effect may be due to an interaction with the matrix. In earlier experiments with the CH_3Cd[21] and CdH[55] radicals the argon matrix $A_{iso}(^{111}Cd)$ values and hence the cadmium 5s character were slightly larger than the neon matrix values. The $3p_z$ character of the HOMO for both the CH_3Mg and MgH radical are also quite similar and their respective $g_\perp$ values, 1.9999(4) for CH_3Mg and 2.0002(4) for MgH,[15] are the same within experimental error which also implies similar $3p_z$ character as the first excitation energy of both radicals are similar. The comparison between the spin densities for both the CH_3Mg and MgH radicals and the MgOH radical shown in Table 4 shows an overall increase in spin density on the magnesium to 99(23)% for MgOH, which is consistent with a larger ionic character to the magnesium−oxygen bond. The major contribution to this increase comes from the increase in the magnesium 3s character which is also consistent with a larger ionic character. This is not surprising given that the hydroxide group is more electronegative than the methyl group.

For further comparison the spin densities determined by a FACM analysis on the metal atoms in the CH_3Zn and CH_3Cd radicals are

$$4s - 0.29(1) \text{ and } 4p_z - 0.56(12)^{22} \text{ for zinc}$$

$$5s - 0.26(1) \text{ and } 5p_z - 0.45(4)^{22} \text{ for cadmium}$$

The p_z orbital character for these two radicals and the CH_3Mg radical are not significantly different however the s orbital character does differ. The dramatically increased metal s orbital character in the CH_3Mg radical compared with the CH_3Zn and CH_3Cd radicals suggests a much more ionic metal−carbon bond in the CH_3Mg radical. This increased ionic character is consistent with the ionization energy for magnesium being lower than that of zinc and cadmium which are similar. The ionic character of the metal−carbon bond will also influence the total spin density on the methyl group. The difficulty of accurately measuring $A_{dip}(^{13}C)$ makes comparison of the ^{13}C values inappropriate however if we assume a similar geometry for the methyl group in these radicals the magnitudes of $A_{iso}(H)$ will be indicative of the spin density on the methyl group. The observed values of 17 MHz for CH_3Cd,[21] 14 MHz for CH_3Zn,[22] and 7 MHz for CH_3Mg follow the expected trend.

There is limited hyperfine detail for the CH_3Ca and CH_3Ba radicals but a comparison with the CH_3Mg radical can still be made with the available data. The hydrogen hyperfine for the CH_3Ca radical has been determined from the pure rotational spectrum using the pump/probe microwave-optical double resonance (PPMODR) technique.[32] The CH_3Ca metal−carbon bond is expected to be more ionic than the magnesium−carbon bond due to the lower ionization energy of calcium. Therefore, the unpaired electron will have a lower spin density on the methyl group in CH_3Ca and a lower hydrogen hyperfine interaction will result if we assume a similar geometry for the methyl group. This proves true when the magnitude of the hydrogen hyperfine parameters are compared for CH_3Mg ($A_{iso}(H) = 7(1)$ MHz) and CH_3Ca (A_{iso} is approximately 2 MHz[32]). The CH_3Ba radical will presumably have an even more ionic bond than the CH_3Ca radical due to the lower ionization energy of barium. The isotropic $A_{iso}(^{137}Ba)$ value for the $^{12}CH_3{}^{137}Ba$ radical has been determined from the pure rotational spectrum.[38] If a FACM analysis is carried out on this value using the theoretical atomic A_{iso} value[41] a barium 6s orbital character of 0.67(1) is obtained for the HOMO. This is substantially higher s character than the magnesium 3s orbital character for the CH_3Mg radical HOMO as expected.

Barckholtz and co-workers have reported "experimental" molecular orbital (MO) diagrams for CH_3Mg and CH_3Zn.[8] The MO diagram was derived from zero kinetic energy pulsed-field ionization (ZEKE-PFI) spectroscopic measurements. The electronic configuration for the CH_3Mg radical is described as $\sigma^2\sigma^{*1}$ where the σ and σ^* orbitals are formed from overlap of the magnesium 3s atomic orbital and the sp^3 hybrid HOMO of the methyl group. This model does not account for the significant amount of magnesium $3p_z$ orbital character in the HOMO of this radical. It is more likely that the HOMO is formed from the overlap of the sp^3 hybrid HOMO of the methyl group and an sp hybrid formed from the magnesium 3s and $3p_z$ atomic orbitals as postulated by Jackson.[56] This would account for the magnesium $3p_z$ orbital character in the CH_3Mg radical HOMO. It is also likely that the bonding molecular orbital, σ will have a greater proportion of the lower energy magnesium 3s atomic orbital and the higher energy σ^* orbital will have a greater proportion of the higher energy magnesium $3p_z$ orbital. The

experimental results seem to justify this assumption. The difference for the magnesium 3s and $3p_z$ orbital characters is not as large as the difference between the zinc 4s and $4p_z$ orbital characters in the CH_3Zn radical. The magnesium 3s and $3p_z$ atomic orbitals are closer in energy than the zinc 4s and $4p_z$ atomic orbitals therefore when they are incorporated into the CH_3Mg radical HOMO they are distributed more evenly between the σ and σ^* molecular orbitals. This along with the greater ionic nature of the magnesium−carbon bond tends to increase the metal s orbital character of the CH_3Mg radical HOMO.

V. Summary

The ^{25}Mg, ^{13}C and D isotopomers of the CH_3Mg radical were generated by the reaction of laser ablated magnesium with various methyl precursors and were isolated in a neon matrix and studied for the first time by ESR spectroscopy. The following magnetic parameters have been derived for the CH_3Mg radical from the matrix ESR results, $g_\perp$, $A_{iso}(^{25}Mg)$, $A_{iso}(^{13}C)$, $A_{iso}(H)$, $A_{dip}(^{25}Mg)$, and $A_{dip}(^{13}C)$. Because of the small size of $A_{dip}(^{25}Mg)$ there was a large error associated with its estimation. These magnetic hyperfine coupling parameters were used to determine the electron spin density distribution for the CH_3Mg radical using the free atom comparison method (FACM). The unpaired electron was found to be largely localized on the magnesium atom and the metal−carbon bonding in this radical was found to be similar to the metal−hydrogen bonding in the MgH radical. The metal bonding in the CH_3Mg radical had a larger ionic character than in the CH_3Zn and CH_3Cd radicals but less ionic than that in the MgOH, CH_3Ca and CH_3Ba radicals.

Ab initio calculations were performed for the CH_3Mg radical. The MP2 level geometry derived for the CH_3Mg radical was consistent with recently reported gas-phase values.[5,7] HFSDCI and MRSDCI calculations of the magnetic hyperfine coupling constants showed a reasonable agreement for the $A_{iso}(^{25}Mg)$, $A_{dip}(^{25}Mg)$ and $A_{dip}(^{13}C)$ values. The agreement for the $A_{iso}(^{13}C)$ was less satisfactory with the HFSDCI value being low by 50% and the MRSDCI value being low by 32%. This discrepancy was attributed to the limited reference space in these calculations resulting in an overestimation of the ionic character of the metal carbon bond. DFT calculations using the UB3LYP and UB3PW91 functionals yielded a geometry with a Mg−C bond length appreciably longer than the experimental value. However the magnetic hyperfine coupling constants calculated with these functionals were in better agreement with the experimental values than those from the CI calculations. Both functionals yielded values for $A_{iso}(^{25}Mg)$, $A_{dip}(^{25}Mg)$ and $A_{dip}(^{13}C)$ in agreement with the experimental values. The value of $A_{iso}(^{13}C)$ from the UB3LYP calculation agreed within the experimental value while that from the UB3PW91 calculation was low by 10%. The theoretical values obtained for $A_{iso}(H)$ from all methods showed poor agreement with experiment.

Acknowledgment. We wish to thank Professor E. R. Davidson (Indiana University) for his help in analyzing why the CI calculations yielded A_{iso} values that differed substantially from the experimental results, Professor T. H. Dunning Jr. (Pacific Northwest National Laboratory) for providing us with his magnesium basis sets, and Professor L. B. Knight Jr. (Furman University) for helpful advice and use of his computing facilities. A.J.M. thanks the Australian Research Council for support of this work under the Small Grants Scheme and The Australian Government Department of Education, Employment, Training and Youth Affairs (DETYA) who provided a Research Infrastructure, Equipment and Facilities Grant that was used to purchase the ESR spectrometer at UWA. E.K. thanks DETYA for an Australian Postgraduate Award with stipend and UWA for a Jean Rogerson Postgraduate Scholarship. Appreciation is expressed to Dr. David Feller and Professor E. R. Davidson for use of their MELDF program for calculating the nuclear hyperfine parameters.

References and Notes

(1) Kawaguchi, K.; Kagi, E.; Hirano, T.; Takano, S.; Saito, S. *Astrophys. J.* **1993**, *406*, L39.
(2) Ziurys, L. M.; Apponi, A. J.; Guélin, M.; Cernicharo, J. *Astrophys. J.* **1995**, *445*, L47.
(3) Ziurys, L. M. *Symp. − Int. Astron. Union* **1997**, *170* (CO: Twenty-Five Years of Millimeter-Wave Spectroscopy), 370.
(4) Lyons, J. R. *Science* **1995**, *267*, 648.
(5) Rubino, R.; Williamson, J. M.; Miller, T. A. *J. Chem. Phys.* **1995**, *103*, 5964.
(6) Salzberg, A. P.; Applegate, B. E.; Miller, T. A. *J. Mol. Spectrosc.* **1999**, *193*, 434.
(7) Anderson, M. A.; Ziurys, L. M. *Astrophys. J.* **1995**, *452*, L157.
(8) Barckholtz, T. A.; Powers, D. E.; Miller, T. A.; Bursten, B. E. *J. Am. Chem. Soc.* **1999**, *121*, 2576.
(9) Bare, W. D.; Andrews, L. *J. Am. Chem. Soc.* **1998**, *120*, 7293.
(10) McCaffrey, J. G.; Parnis, J. M.; Ozin, G. A.; Breckenridge, W. H. *J. Phys. Chem.* **1985**, *89*, 4945.
(11) Quelch, G. E.; Hillier, I. H. *J. Chem. Soc., Faraday Trans. 2* **1987**, *83*, 1637.
(12) Kaupp, M.; Stoll, H.; Preuss, H. *J. Comput. Chem.* **1990**, *11*, 1029.
(13) Gardner, P. J.; Preston, S. R.; Siertsema, R.; Steele, D. *J. Comput. Chem* **1993**, *14*, 1523.
(14) Woon, D. E. *J. Chem. Phys.* **1996**, *104*, 9495.
(15) Knight, L. B., Jr.; Weltner, W., Jr. *J. Chem. Phys.* **1971**, *54*, 3875.
(16) Knight, L. B., Jr.; Easley, W. C.; Weltner, W., Jr.; Wilson, M. *J. Chem. Phys.* **1971**, *54*, 322.
(17) Brom, J. M.; Weltner, W., Jr. *J. Chem. Phys.* **1973**, *58*, 5322.
(18) Anderson, M. A.; Allen, M. D.; Ziurys, L. M. *J. Chem. Phys.* **1994**, *100*, 824.
(19) Barclay, W. L., Jr.; Anderson, M. A.; Ziurys, L. M. *Chem. Phys. Lett.* **1992**, *196*, 225.
(20) Ziurys, L. M.; Barclay, W. L., Jr.; Anderson, M. A. *Ap. J. Lett.* **1993**, *402*, L21.
(21) Karakyriakos, E.; Davis, J. R.; Wilson, C. J.; Yates, S. A.; McKinley, A. J.; Knight, L. B., Jr.; Babb, R.; Tyler, D. J. *J. Chem. Phys.* **1999**, *110*, 3398.
(22) McKinley, A. J.; Karakyriakos, E.; Knight, L. B., Jr.; Babb, R.; Williams, A. *J. Phys. Chem. A* **2000**, *104*, 3528.
(23) Knight, L. B., Jr.; Herlong, J. O.; Cobranchi, S. T.; Kirk, T. *J. Chem. Phys.* **1990**, *92*, 6463.
(24) Knight, L. B., Jr.; Cobranchi, S. T.; Petty, J.; Cobranchi, D. P. *J. Chem. Phys.* **1989**, *91*, 4587.
(25) Ozin, G. A.; McCaffrey, J. G.; Parnis, J. M. *Angew. Chem., Int. Ed. Engl.* **1986**, *25*, 1072.
(26) Knight, L. B., Jr.; Banisaukas, T. J., III; Babb, R.; Davidson, E. R. *J. Chem. Phys.* **1996**, *105*, 6607.
(27) Parnis, J. M.; Ozin, G. A. *J. Phys. Chem.* **1989**, *93*, 1204.
(28) Li, B.-Z.; Xin, J.; Ziurys, L. M. *Chem. Phys. Lett.* **1997**, *280*, 513.
(29) Tan, X. Q.; Cerny, T. M.; Williamson, J. M.; Miller, T. A. *J. Chem. Phys.* **1994**, *101*, 6396.
(30) Cerny, T. M.; Tan, X. Q.; Williamson, J. M.; Robles, E. S. J.; Ellis, A. M.; Miller, T. A. *J. Chem. Phys.* **1993**, *99*, 9376.
(31) Panov, S. I.; Powers, D. E.; Miller, T. A. *J. Chem. Phys.* **1998**, *108*, 1335.
(32) Namiki, K. C.; Steimle, T. C. *J. Chem. Phys.* **1999**, *110*, 11309.
(33) Brazier, C. R.; Bernath, P. F. *J. Chem. Phys.* **1989**, *91*, 4548.
(34) Marr, A. J.; Grieman, F.; Steimle, T. C. *J. Chem. Phys.* **1996**, *105*, 3930.
(35) Anderson, M. A.; Ziurys, L. M. *Astrophys. J. Lett.* **1996**, *460*, L77.
(36) Anderson, M. A.; Robinson, J. S.; Ziurys, L. M. *Chem. Phys. Lett.* **1996**, *257*, 471.
(37) Brazier, C. R.; Bernath, P. F. *J. Chem. Phys.* **1986**, *86*, 5918.
(38) Xin, J.; Robinson, J. S.; Apponi, A. J.; Ziurys, L. M. *J. Chem. Phys.* **1998**, *108*, 2703.
(39) Knight, L. B., Jr.; Steadman, J.; Miller, P. K.; Cleveland, J. A., Jr. *J. Chem. Phys.* **1988**, *88*, 2226.
(40) Knight, L. B., Jr.; Cobranchi, S. T.; Earl, E. *J. Chem. Phys.* **1988**, *88*, 7348.
(41) Weltner, W., Jr. *Magnetic Atoms and Molecules*; Van Nostrand Reinhold: New York, 1983.

(42) MELDF was originally written by L. McMurchie, S. Elbert, S. Langoff, E. R. Davidson. It has been substantially modified by D. Feller, R. Cave, D. Rawlings, R. Frey, R. Daasch, L. Mitzche, P. Phillips, K. Iberle, C. Jackels, E. R. Davidson.

(43) Frisch, M. J.; Trucks, G. W.; Schlegel, H. B.; Gill, P. M. W.; Johnson, B. G.; Robb, M. A.; Cheeseman, J. R.; Keith, T.; Petersson, G. A.; Montgomery, J. A.; Raghavachari, K.; Al-Laham, M. A.; Zakrzewski, V. G.; Ortiz, J. V.; Foresman, J. B.; Cioslowski, J.; Stefanov, B. B.; Nanayakkara, A.; Challacombe, M.; Peng, C. Y.; Ayala, P. Y.; Chen, W.; Wong, M. W.; Andres, J. L.; Replogle, E. S.; Gomperts, R.; Martin, R. L.; Fox, D. J.; Binkley, J. S.; Defrees, D. J.; Baker, J.; Stewart, J. P.; Head-Gordon, M.; Gonzalez, C.; Pople, J. A. *Gaussian 94*, Revision D.2; Gaussian, Inc.: Pittsburgh, PA, 1995.

(44) Frisch, M. J.; Trucks, G. W.; Schlegel, H. B.; Scuseria, G. E.; Robb, M. A.; Cheeseman, J. R.; Zakrzewski, V. G.; Montgomery, J. A., Jr., Stratmann, R. E.; Burant, J. C.; Dapprich, S.; Millam, J. M.; Daniels, A. D.; Kudin, K. N.; Strain, M. C.; Farkas, O.; Tomasi, J.; Barone, V.; Cossi, M.; Cammi, R.; Mennucci, B.; Pomelli, C.; Adamo, C.; Clifford, S.; Ochterski, J.; Petersson, G. A.; Ayala, P. Y.; Cui, Q.; Morokuma, K.; Malick, D. K.; Rabuck, A. D.; Raghavachari, K.; Foresman, J. B.; Cioslowski, J.; Ortiz, J. V.; Baboul, A. G.; Stefanov, B. B.; Liu, G.; Liashenko, A.; Piskorz, P.; Komaromi, I.; Gomperts, R.; Martin, R. L.; Fox, D. J.; Keith, T.; Al-Laham, M. A.; Peng, C. Y.; Nanayakkara, A.; Gonzalez, C.; Challacombe, M.; Gill, P. M. W.; Johnson, B.; Chen, W.; Wong, M. W.; Andres, J. L.; Gonzalez, C.; Head-Gordon, M.; Replogle, E. S.; Pople, J. A. *Gaussian 98*, Revision A.7; Gaussian, Inc.: Pittsburgh, PA, 1998.

(45) Knight, L. B., Jr.; King, G. M.; Petty, J. T.; Matsushita, M.; Momose, T.; Shida, T. *J. Chem. Phys.* **1995**, *103*, 3377.

(46) Personal communication. Professor T. H. Dunning, Jr. Pacific National Laboratory.

(47) Dunning, T. H., Jr.; Hay, P. J. In *Methods of Electronic Structure Theory*; Schaefer, H. F., III, Ed.; Plenum Press: New York, 1977; Vol 2.

(48) Becke, A. D. *J. Chem. Phys*. **1993**, *98*, 5648.

(49) Burke, K.; Perdew, J. P.; Wang, Y. In *Electronic Density Functional Theory: Recent Progress and New Directions*; Dobson, J. F., Vignale, G., Das, M. P., Eds.; Plenum Press: New York, 1998.

(50) Moore, C. E. *Atomic Energy Levels*; NBS: Washington, DC, 1949; Vol. 1.

(51) Knight, L. B., Jr.; Lin, K. C. *J. Chem. Phys.* **1972**, *56*, 6044.

(52) Kluge, H.-J.; Sauter, H. *Z. Phys.* **1974**, *270*, 295.

(53) Ammeter, J. H.; Schlosnagle, D. C. *J. Chem. Phys.* **1973**, *59*, 4784.

(54) Bauche, J.; Couarraze, G.; Labarthe, J.-J. *Z. Physik* **1974**, *270*, 311.

(55) Knight, L. B., Jr.; Miller, P. K.; Steadman, J. *J. Chem. Phys.* **1984**, *80*, 4587.

(56) Jackson, R. L. *J. Chem. Phys*. **1990**, *174*, 53.